# Light-induced Reorientation in the Purple Membrane

Chaozhi Wan, Jun Qian, and Carey K. Johnson
Department of Chemistry, University of Kansas, Lawrence, Kansas 66045 USA

ABSTRACT Reorientation of bacteriorhodopsin in the native purple membrane was studied by time-resolved linear dichroism spectroscopy (TRLD) over the millisecond time regime. The time responses observed in TRLD are distinctly different from the isotropic transient absorption (TA) at wavelengths in the range 550–590 nm, where the bacteriorhodopsin ground state absorbs. In contrast, the TA and TRLD responses have nearly identical time dependence at 410 and 690 nm, where the intermediates M and O, respectively, principally contribute. These results demonstrate ground-state bacteriorhodopsin reorientation triggered by the photocycle. The TRLD and TA data are analyzed to test models for reorientational motion. Rotational diffusion of ground-state bacteriorhodopsin cannot account for the details of the data. Rather, the results are shown to be consistent with a reversible reorientation of "spectator" (nonexcited) members of the bacteriorhodopsin trimer in the purple membrane in response to the photocycling member of the trimer. This response may be associated with cooperativity in the trimer.

## INTRODUCTION

Bacteriorhodopsin (BR), a photoactive membrane protein found in the purple membrane (PM) of *Halobacterium halobium*, transduces light energy into chemical potential by pumping protons across the cell membrane. BR is embedded in the purple membrane of *H. halobium* and organized in trimeric unit cells arranged in a hexagonal two-dimensional lattice. The protein (molecular weight 26,000) constitutes 75% of the total mass, with lipid making up the remaining 25% of the purple membrane. A retinal Schiff base covalently linked to each protein in a 1:1 ratio is responsible for light absorption, which initiates a photochemical *trans* to *cis* isomerization within 1 ps of excitation. The sequence of ground-state transient intermediates which follows, BR→J→K→L→M→N→O→BR, constitutes the bacteriorhodopsin photocycle (for recent reviews, see Refs. 1 and 2). The J→K step involves picosecond ground-state relaxation or vibrational cooling. In the K→L step, the chromophore relaxes to a planar 13-*cis* configuration in roughly 1 μs. The formation of M occurs as the retinal Schiff base deprotonates. Since Asp-85 is protonated simultaneously (3, 4), it apparently serves as the corresponding proton acceptor. The Schiff base is reprotonated in the M→N step (5), apparently from Asp-96 (6–8). The all-*trans* conformation of the retinal Schiff base is restored with the formation of the O intermediate (9), while a proton is taken from the cytoplasmic side of the membrane and Asp-96 is reprotonated (7, 10).

Protein conformational changes have been proposed to play a vital functional role in the proton transport mechanism in several recent models (1, 5, 11). The possibility of conformational changes in the M and N intermediates has been investigated in detail by resonance Raman spectroscopy (5), Fourier transform infrared (FTIR) spectroscopy (3, 12), and time-resolved absorption measurements (13, 14). Recent neutron diffraction and time-resolved x-ray diffraction studies have shown that, after a light-induced change of the tertiary structure of BR generated during the BR to M transition, BR relaxes to its original conformation during the M to BR transition as BR regains its crystalline structure (15, 16). Studies of the reactivity of wild-type and mutant strains of BR with hydroxylamine also indicate an internal conformational change induced by light absorption (17).

Orientational motion in the PM has also been investigated, principally by linear dichroism spectroscopy, which detects reorientation of the retinal chromophore following polarization-selective excitation of BR (18–23). Some of these studies have detected reorientation in BR during the M→N→O→BR transition (18, 19, 22, 23). Ahl and Cone (22) attributed orientational motion observed with ~1-ms resolution in PM suspensions to the rotation of monomeric proteins within the trimer in the BR membrane. Studies of BR in gels (agar or polyacrylamide), on the other hand, have not detected orientational motion (21, 24, 25).

Recently orientational motion in BR has been studied in our laboratory by time-resolved polarization spectroscopy (26) and time-resolved linear dichroism (TRLD) spectroscopy (23) with ~50-ps resolution. Reorientation associated with the K→L transition was observed. Since *trans* → *cis* isomerization itself causes little change in the orientation of the transition dipole, this observation represents a reorientation of the chromophore apparently associated with either a protein conformational change or rotation of the protein.

In the present work, we have studied the orientational motion in BR during the M→N→O→BR transitions by TRLD at room temperature and low temperature (3°C), and as a function of solvent. Possible orientational motions are discussed in the context of the trimeric lattice structure of BR in the membrane.

*Received for publication 4 February 1993 and in final form 30 April 1993.*
Address reprint requests to C. K. Johnson

0006-3495/93/08/927/12 $2.00

## EXPERIMENTAL PROCEDURES

The experimental arrangement, diagrammed in Fig. 1, is identical to that described previously (23). Glan Taylor polarizers (Karl Lambrecht Corp., Chicago, IL) were used to polarize and analyze the probe pulses. The pump

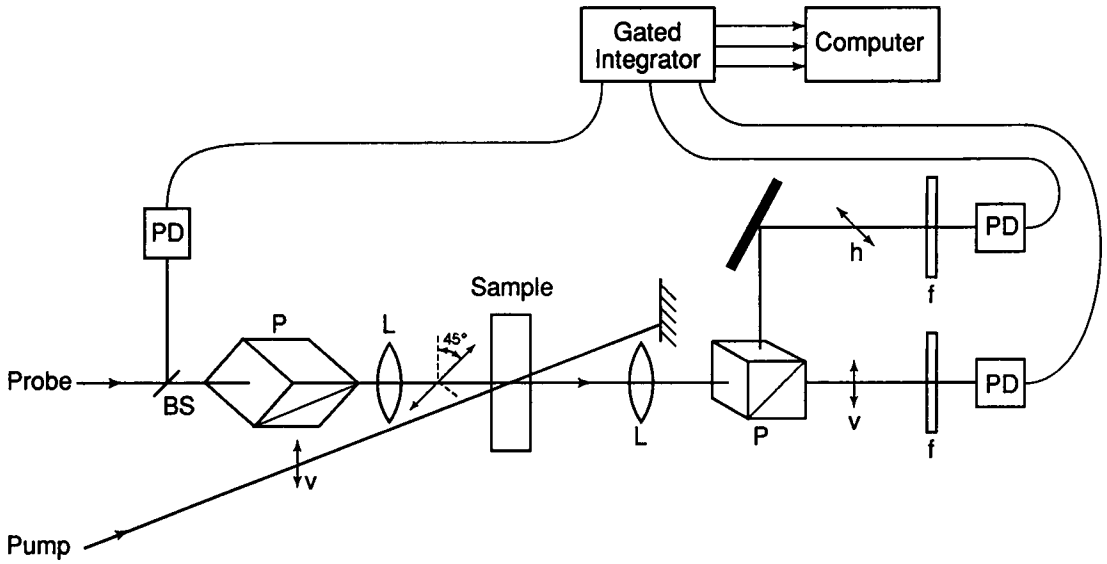


FIGURE 1 Experimental arrangement for time-resolved linear dichroism experiments. PD, photodiode; BS, beam splitter; L, lens; P, polarizer; f, filter; h, horizontal; and v, vertical polarization. The polarizer to the left of the sample ($P_{pr}$ in text) selects the probe polarization 45° from vertical, and the analyzing polarizer to the right of the sample ($P_{an}$) separates the vertical and horizontal components.

beam was polarized vertically, and the probe beam was oriented at 45° with respect to the pump polarization. The analyzing polarizer was oriented to select vertical and horizontal components of the probe beam of equal intensity when the pump beam was blocked. Since inadequate alignment of the polarizers can result in systematic errors in anisotropy values, special care was taken to assure precise alignment of the two probe-beam polarizers, $P_{pr}$ and $P_{an}$, where $P_{pr}$ is the polarizer preceding the sample, set at 45° from vertical, and $P_{an}$ is the analyzing polarizer following the sample. These polarizers were mounted in high resolution rotation stages (6-arc-s resolution). They were set as follows. $P_{an}$ was first adjusted to be parallel (±0.05°) to the pump polarization by rotating it to achieve minimum intensity of the rejected pump beam. This defines 0° for $P_{an}$. Then, $P_{an}$ was rotated by precisely 45°, and $P_{pr}$ was adjusted to extinguish the transmitted probe beam. This sets $P_{pr}$ to transmit light polarized at 45° with respect to the pump polarization. Finally, $P_{an}$ was returned to 0° to separate the vertical and horizontally polarized components of the probe beam. The result is the orientation of polarizers shown in Fig. 1. The pump-pulse polarization and the analyzing polarizer are aligned to within ≤0.5° by this method.

The excitation pulse energy in these experiments was less than 2 μJ at 568 nm, while the energy of the probe pulses was limited to less than 0.02 μJ with neutral optical density filters. The focused beam diameter of both the pump and probe beams was about 0.6 mm. Under these conditions, <10% of BR molecules in the probed volume were excited, and in only 3% of trimers were more than one monomer excited. The laser system consisting of dual picosecond dye lasers pumped by synchronized mode-locked, Q-switched CW ND:YAG lasers (27), generates pump and probe pulses of about 50-ps duration with time delays between pump and probe variable from the picosecond to the second time scales. The pump pulse repetition rate was 2–30 Hz, selected so that the time between two sequential pump pulses was longer than the photocycle completion time. The probe repetition rate was 30–400 Hz. For long time scans, the sample was probed up to 100 times for each pump pulse.

The probe signals with polarizations parallel (vertical) and perpendicular (horizontal) to the excitation pulse were detected by large-area photodiodes. The probe pulse intensity was also sampled by another photodiode to generate a reference signal. Parallel, perpendicular, and reference signals were processed by gated integrators. Both the parallel and perpendicular signals were divided by the reference signal to compensate for pulse-to-pulse fluctuations, and the resulting ratios were digitized and stored in a computer for analysis.

The purple membrane was extracted from *H. halobium* strain ET1-001 by standard methods (28) and suspended in phosphate buffer at pH 7. The glutaraldehyde-fixed membrane was prepared by the method of Ahl and Cone (22). The sample was light-adapted by exposure to a 100-watt lamp. Light adaptation was verified by the shift in the absorption maximum from 558 nm in dark-adapted BR to 568 nm in light-adapted BR. The sample was flowed through a 2.5-mm thick sample cell at a rate of from 1 to 4 mm/s. The temperature was controlled by a thermostated water bath, which also circulated through the sample mount to prevent sample warming as it circulated through the sample cell in low temperature experiments. The optical density of the sample in the sample cell was about 1 at 568 nm.

## RESULTS

Light-adapted BR was excited at 568 nm. Time-dependent absorption signals parallel, $\Delta A_{\parallel} = \log(I_0/I_{\parallel})$, and perpendicular, $\Delta A_{\perp} = \log(I_0/I_{\perp})$, to the pump polarization were measured at probe wavelengths from 410 to 690 nm. The time-resolved linear dichroism, $D(t) = \Delta A_{\parallel} - \Delta A_{\perp}$, the total isotropic transient absorption (TA),[1] $\Delta A(t) = \Delta A_{\parallel} + 2\Delta A_{\perp}$, and the anisotropy, $r(t) = (\Delta A_{\parallel} - \Delta A_{\perp})/(\Delta A_{\parallel} + 2\Delta A_{\perp})$, were calculated from the digitized signals. Parallel and perpendicular absorption signals were measured simultaneously as described previously (23) to allow precise comparison of the transient absorption and linear dichroism. The TRLD signal is dependent on orientation, while the TA signal is rotation-independent. The differences between the time-dependent decays of the TRLD and the TA therefore yield information about orientational motions of bacteriorhodopsin.

### Data analysis

We have used two approaches to analyze our data. The first is directly to plot and fit the anisotropy $r(t)$. The second is

[1] Hereafter we refer to $\Delta A(t)$ as defined here as the transient absorption (TA). The isotropic transient absorption that would be measured at the magic angle (54.7°) is one-third of the TA defined here.

to analyze the linear dichroism $D(t)$ and to compare it with the transient absorption $\Delta A(t)$ to obtain the rotational time. In principle, both methods should give the same result. In practice one method may be more suitable than the other. The anisotropy $r(t)$ describes the rotational motion well if only one transition is detected, as in many anisotropic fluorescence studies and in linear dichroism studies of dye molecules. However, for a complex system such as BR in which the absorption bands of several species overlap each other over a broad wavelength range, the anisotropy may not be the most useful function to describe the rotational motion for several reasons. First, the transient absorption $\Delta A(t)$ may go through zero, resulting in a singularity in the anisotropy. For example, at 640 nm (data not shown) the transient absorption is first dominated by the negative intensity of the BR "hole," and then increases, goes through zero, and finally becomes positive during the formation of the O intermediate.

Second, we find that small changes in the alignment of the polarizers can influence the measured anisotropy. We have repeatedly measured the TA and TRLD at a probe wavelength of 410 nm at 25°C, and have found that small changes in the polarization angle within ± 0.5° can change the time dependence of the anisotropy at long times (>4 ms), when the population of the M intermediate becomes small. This effect is caused by the overlapping contributions of M410 and BR570 and can be understood as follows. Since the contribution of BR570 to the TA at 410 nm is negative, the TA will approach zero and may even become negative as M410 decays. Although the pump and analyzer polarization are aligned to better than ± 0.5°, any slight misalignment of the analyzing polarizer with respect to the pump polarization will result in a small degree of mixing of $\Delta A_{\parallel}$ and $\Delta A_{\perp}$ signals. While the resulting experimental error in the TRLD is small, it is magnified in the anisotropy plot as $\Delta A$ approaches zero. The fits to the TRLD and TA decays, on the other hand, are not sensitive to polarizer alignment.

Third, the anisotropy is very sensitive to noise in the measuring process, especially, for times longer than twice the population decay times. The dichroism, on the other hand, is less affected by these problems. For example, as the probe polarization angle changes within ± 0.5°, the TRLD lifetime at 410 nm does not change within our experimental error (Table 1). Therefore, in this work, we have obtained the rotational times by fitting the TRLD and TA separately, rather than from fits to the anisotropy $r(t)$.

**TABLE 1 Lifetimes of BR measured at 25°C***

| | λ | $\tau_{LD}$ | $\tau_{TA}$ | $\tau_r$‡ |
|---|---|---|---|---|
| | nm | ms | ms | ms |
| In pH 7 buffer | 410 | 2.22 ± 0.08 | 2.32 ± 0.14 | |
| | 410 | 212 ± 0.06 | 2.15 ± 0.06 | |
| | 550 | 2.87 ± 0.06 | 4.29 ± 0.16 | 8.77 |
| | 570 | 2.23 ± 0.14 | 4.00 ± 0.14 | 5.0 |
| | 590 | 2.51 ± 0.06 | 4.12 ± 0.08 | 6.4 |
| | 640 | 1.75 ± 0.24 | 1.84 ± 0.34 | |
| | | 5.41 ± 0.8 | 4.81 ± 1.0 | |
| | 690 | 1.49 ± 0.5 | 1.24 ± 0.5 | |
| | | 5.11 ± 1.4 | 5.22 ± 1.7 | |
| In 40% glycerol | 410 | 11.8 ± 1.2 | 11.4 ± 2.0 | |
| | 570 | 7.76 ± 0.16 | 11.2 ± 0.2 | 25 |
| | 640 | 5.96 ± 3.8 | 6.05 ± 8 | |
| | | 7.10 ± 4.5 | 7.28 ± 9.6 | |
| In 80% glycerol | 410 | 2.97 ± 0.12 | 2.97 ± 0.4 | |
| | | 31.8 ± 0.6 | 33.1 ± 1.6 | |
| | | 42.2 ± 1.6 | 54.4 ± 2.0 | 188 |
| Fixed with glutaraldehyde | 410 | 2.58 ± 0.26 | 4.50 ± 0.8 | |
| | | 35.2 ± 0.4 | 45.1 ± 1.6 | 160 |
| | 570 | 12.6 ± 1.4 | 17.8 ± 1.6 | 43 |
| | | 47.0 ± 1.6 | 53.2 ± 2.2 | 481 |

* Errors reported are two times the standard deviations in the least-squares fitting parameters.
‡ $\tau_r = (1/\tau_{LD} - 1/\tau_{TA})^{-1}$.

## Measurements at room temperature

Figs. 2, 3, and 4 show the anisotropy, TA, and TRLD decays at 25°C at probe wavelengths of 550, 570, and 590 nm, respectively. These scans contain contributions both from the BR ground-state bleaching and the N intermediate. The anisotropies are strongly wavelength-dependent. For comparison, the experimentally determined anisotropy, TA, and TRLD at 410 and 690 nm are shown in Figs. 5 and 6. At 410 and 690 nm the anisotropy is nearly constant over the 10-ms time range (Figs. 5 and 6), while at 550–590 nm, anisotropy decay is observed over this time range. Generally similar anisotropy decays were observed at 400, 570, and 650 nm for BR at 30°C by Ahl and Cone (22), although they found a more marked anisotropy increase at 400 nm between 2 and 10 ms. As discussed above, we have obtained similar anisotropy behavior at 410 nm by small changes in polarization angle.

If reorientational motion occurs during the population decay time for a species absorbing at any of the wavelengths probed, the TRLD response will differ from the TA (23). Specifically, a faster decay is expected for TRLD than for TA (see Discussion). To obtain the lifetimes of TA and TRLD signals, we fitted the data measured at 410, 550, 570, and 590 nm with single exponential functions and at 640 and 690 nm with two exponential functions, respectively. (Double exponential functions were used at 640 and 690 nm, since it is necessary to account for the rise and decay of the population of the O intermediate.) The resulting time constants are shown in Table 1. For M (at 410 nm), the TA and TRLD signals decay with the same lifetime within experimental error. The same is true for O (at 690 nm). In contrast, the lifetimes at 550, 570, and 590 nm in the TRLD decays are much shorter than in the TA decays. If the reorientation can be described by an exponential decay (e.g., rotational diffusion), then

$$D(t) = \Delta A(t) r(0) e^{-t/\tau_r} \quad (1)$$

where $\tau_r$ is the rotational time constant. Hence, for exponential fits to $D(t)$ and $\Delta A(t)$, $\tau_r$ can be calculated from the measured time constants by

$$\tau_r = \left( \frac{1}{\tau_{LD}} - \frac{1}{\tau_{TA}} \right)^{-1} \quad (2)$$

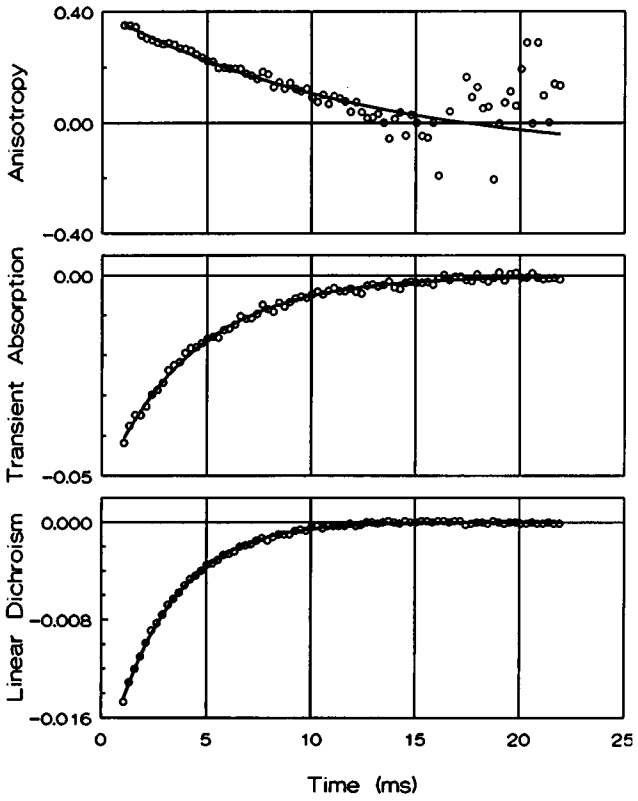


FIGURE 2 Anisotropy (*top*), transient absorption (*center*), and time-resolved linear dichroism (*bottom*) of bacteriorhodopsin measured at 550 nm at 25°C. Experimental data are plotted as open circles. The solid lines are least-squares fits to the data. The anisotropy and TRLD plots are fit to Eqs. 13 and 14, respectively. The TA data are fit to a single-exponential function with the time constant in Table 1.

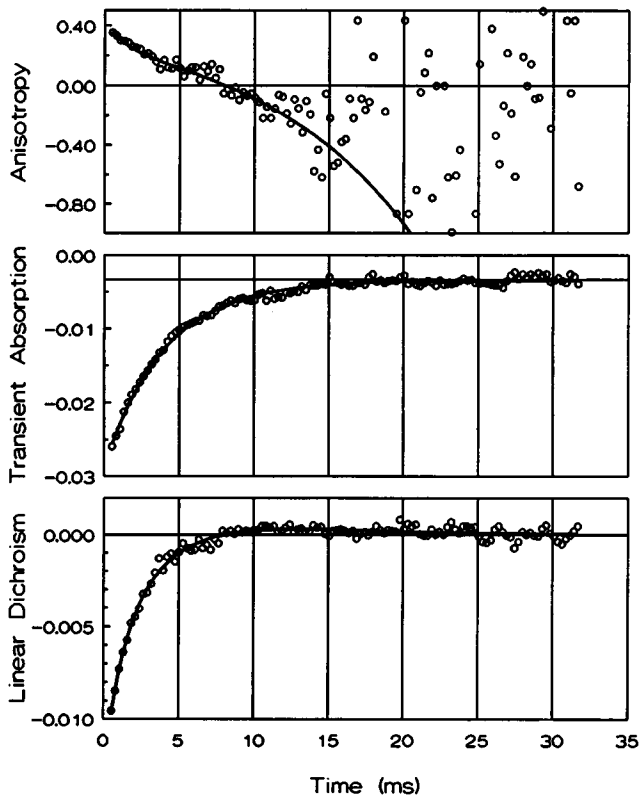


FIGURE 3 Anisotropy (*top*), transient absorption (*center*), and time-resolved linear dichroism (*bottom*) of bacteriorhodopsin measured at 570 nm at 25°C. Experimental data are plotted as open circles. The solid lines are least-squares fits to the data. The anisotropy and TRLD plots are fit to Eqs. 13 and 14, respectively. The TA data are fit to a single-exponential function (time constant in Table 1).

where $\tau_{LD}$ and $\tau_{TA}$ are the time constants in TRLD and TA decays, respectively. The rotational time constant $\tau_r$ obtained for scans at 550, 570, and 590 nm is about 6–9 ms (see Table 1), while for scans at 640 and 690 nm, $\tau_r$ is longer than 50 ms (much longer than the measured decays), indicating no measurable reorientation within experimental accuracy.

An unusual feature in the TRLD response at 570 and 590 nm is the positive linear dichroism at times longer than 9 ms (at 570 nm) and 10 ms (at 590 nm). Since the TA is negative due to the bleaching of BR absorption, this corresponds to a negative anisotropy at long times.

## Solvent dependence

The solvent dependence of reorientation times was investigated in a series of measurements for bacteriorhodopsin in glycerol/water solution. Glycerol was added to BR solution to obtain 40 and 80% by volume glycerol/water mixtures, and the TA and TRLD signals were measured at 25°C. The results (Table 1) again show no detectable reorientational motion at probe wavelengths of 410 and 640 nm, while reorientation times of 25 and 188 ms were measured at a probe wavelength of 570 nm for 40 and 80% glycerol/water mixtures, respectively. Both the reorientation time $\tau_r$ as well as $\tau_{TA}$ and $\tau_{LD}$ increase as the percentage of glycerol increases.

The reorientational motion observed above cannot be attributed to overall rotation of membrane fragments because the overall rotation of membrane is expected to be much slower (22) and should be wavelength-independent. Rotational diffusion of membrane fragments on a time scale comparable to the photocycling time (~4 ms) would cause anisotropy decay at 410 and 690 nm as well as 550–590 nm, contrary to our observations. Since glutaraldehyde can cross-link the proteins in the purple membrane fragments and eliminate the motion of BR monomers inside the membrane, the overall rotational time of membrane fragments was obtained by glutaraldehyde fixation, following Ahl and Cone (22). The measured lifetimes of TA and TRLD for the glutaraldehyde-fixed protein at 410 nm at 25°C are 45 and 35 ms, respectively, corresponding to an overall rotational time of 160 ms of membrane fragments. (The fast time constant at 410 nm is the rise time of the M intermediate. Since this time constant is comparable to the step time for these scans, we do not regard the difference in the fast time constant obtained in the fits to the TA and TRLD scans to be significant.) The decay times at 570 nm in glutaraldehyde-fixed sample also indicate a rotational time longer than the photocycle time, although, since the appearance and decay times of the bleach are of the same order of magnitude, it is not possible to extract the two time constants reliably by least-squares fitting. Conse-

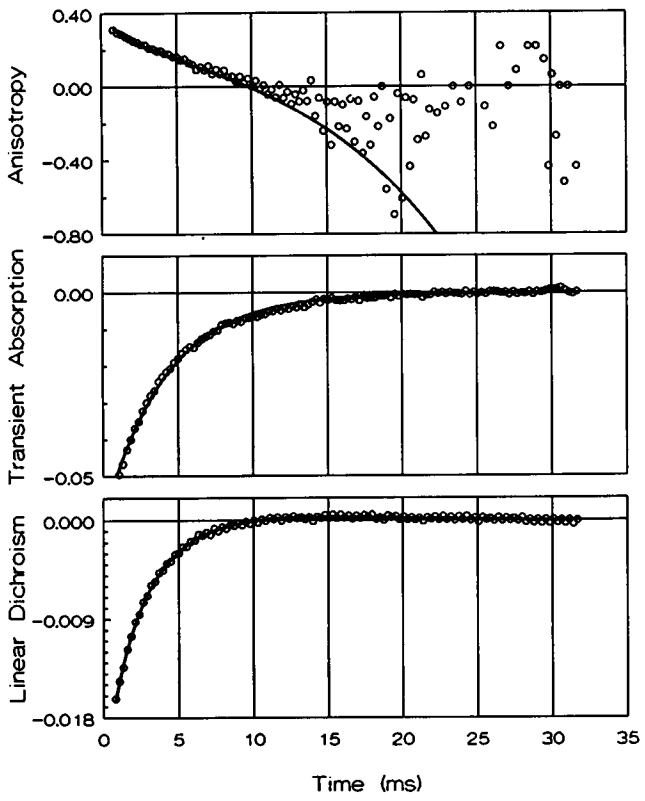


FIGURE 4 Anisotropy (*top*), transient absorption (*center*), and time-resolved linear dichroism (*bottom*) of bacteriorhodopsin measured at 590 nm at 25°C. Experimental data are plotted as open circles. The solid lines are least-squares fits to the data. The anisotropy and TRLD plots are fit to Eqs. 13 and 14, respectively. The TA data are fit to a single-exponential function (time constant in Table 1).

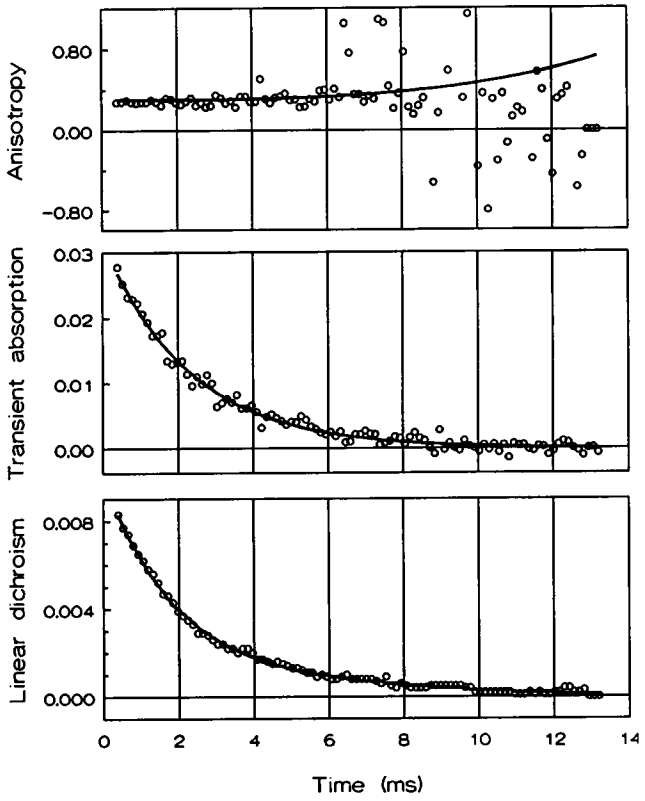


FIGURE 5 Anisotropy (*top*), transient absorption (*center*), and time-resolved linear dichroism (*bottom*) of bacteriorhodopsin measured at 410 nm at 25°C. Experimental data are plotted as open circles. The solid lines are least-squares fits to the data. The anisotropy and TRLD plots are fit to Eqs. 13 and 14, respectively. The TA data are fit to a single-exponential function (time constant in Table 1).

quently, a large variation is seen in the rotational time constants in Table 1 for glutaraldehyde-treated samples. The glutaraldehyde-treated sample may also exhibit inhomogenous kinetics. However, it is clear that the overall rotation of membrane fragments is too slow to be detected during the normal course of the photocycle at room temperature.

## Temperature dependence

Since orientational motion is temperature-dependent, decays were also recorded at a temperature of 3°C. Figs. 7 and 8 show the low-temperature TA and TRLD decays at 410 and 570 nm, respectively. The time constants for TA are clearly different from those for TRLD at wavelengths of both 410 and 570 nm at this temperature. The resulting calculated reorientation times $\tau_r$ are 169 and 80 ms at 410 and 570 nm, respectively (see Table 2). We also measured the overall rotational time of the glutaraldehyde-fixed membrane at 3°C and obtained a membrane rotational time of about 260 ms. Since the overall rotational times $\tau_r$ are shorter than the membrane rotational time $\tau_m$, there must be an additional rotational component with rotational time $\tau_s$. If the measured rotational time is written $\tau_r = (1/\tau_m + 1/\tau_s)^{-1}$, we obtain 372 and 109 ms for $\tau_s$ at 410 and 570 nm, respectively. Thus, in contrast to the situation at room temperature, one must consider the membrane rotation at low temperature, where $\tau_r$ is of the same order as $\tau_m$.

The rotational constant in rotational diffusion is expected to be proportional to the viscosity (29). The temperature dependence of rotational times in glutaraldehyde-fixed samples shows that the rotational diffusion time constants $\tau_m$ of membrane particles increases by a factor of ~1.6 when the temperature is lowered from 25 to 3°C. This is consistent with the temperature dependence of water viscosity, which increases by a factor of 1.8 over the same temperature range (30). In contrast, the rotational time $\tau_r$ measured at 550–590 nm exhibits a much stronger temperature dependence, increasing by more than a factor of 10 from ~7 to 80 ms between 25 and 3°C. Hence, the rotational decay times measured at 550–590 nm are inconsistent with rotational diffusion in water.

## DISCUSSION

Since bacteriorhodopsin is a multilevel system, several states contribute significantly to the observed TA, TRLD, and anisotropy. These signals can be written

$$\Delta A_\lambda(t) = \Delta A_\lambda^{BR}(t) + \sum_i \Delta A_\lambda^i(t) \qquad (3)$$

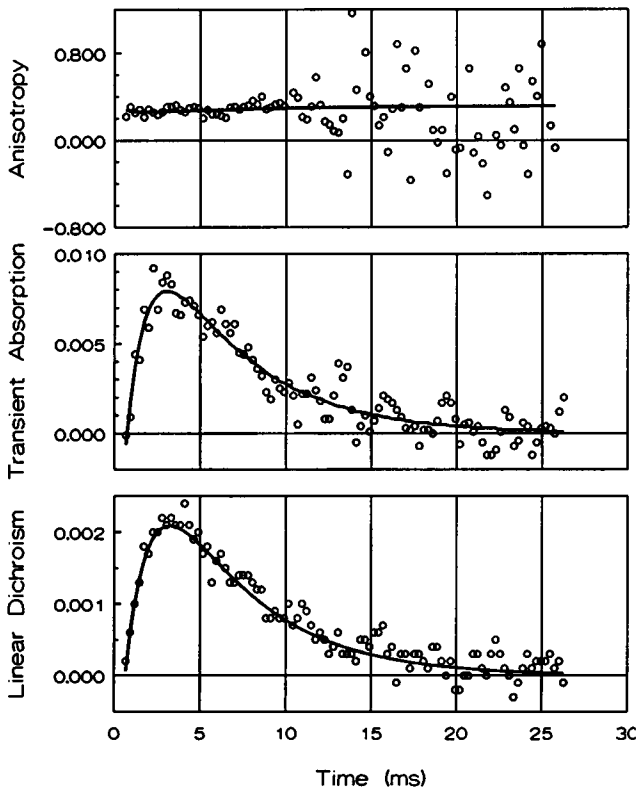


FIGURE 6 Anisotropy (*top*), transient absorption (*center*) and time-resolved linear dichroism (*bottom*) of bacteriorhodopsin measured at 690 nm at 25°C. Experimental data are plotted as open circles. The solid lines are least-squares fits to the data. The anisotropy and TRLD plots are fit to Eqs. 13 and 14, respectively. The TA data are fit to a double-exponential function (time constants in Table 1).

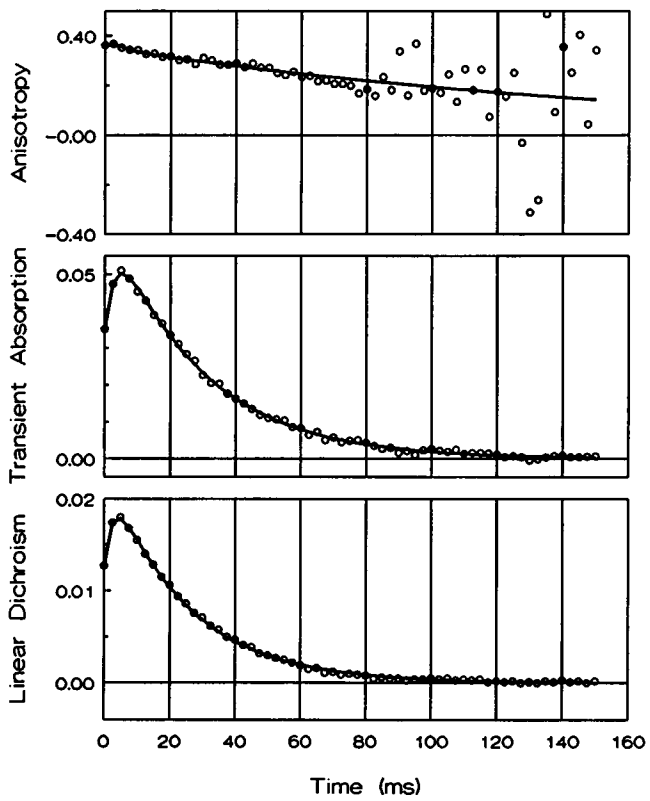


FIGURE 7 Anisotropy (*top*), transient absorption (*center*), and time-resolved linear dichroism (*bottom*) of bacteriorhodopsin measured at 410 nm at 3°C. The solid lines are least-squares fits to the data. The anisotropy and TRLD plots are fit to Eqs. 13 and 14, respectively. The TA data are fit to a double-exponential function (time constants in Table 2).

$$D_\lambda(t) = \Delta A_\lambda^{BR}(t) r_{BR}(t) + \sum_i \Delta A_\lambda^i(t) r_i(t) \quad (4)$$

$$r_\lambda(t) = \frac{\Delta A_\lambda^{BR}(t)}{\Delta A_\lambda(t)} r_{BR}(t) + \sum_i \frac{\Delta A_\lambda^i(t)}{\Delta A_\lambda(t)} r_i(t) \quad (5)$$

where $\Delta A_\lambda^{BR}(t)$ and $\Delta A_\lambda^i(t)$ are the absorbance changes of BR and intermediate $i$ at wavelength $\lambda$ and $r_{BR}(t)$ and $r_i(t)$ are the anisotropies of the BR hole and the intermediate $i$, respectively. (The term "hole" is used here for the orientationally anisotropic BR570 population remaining after excitation by the pump pulse.)

At some wavelengths, more than one intermediate contributes to the absorption and dichroism signals. In this case, Eqs. 3–5 include contributions from several components. It follows that the wavelength-dependence of the anisotropy, $r_\lambda(t)$, can be quite complex and cannot be described simply by a two-population model. Such an analysis was used in Ref. 22, where only BR570 and M410 or O640 populations were considered in the analysis of anisotropies in BR. Recent Raman and transient absorption studies have fit a sequence BR→K↔L↔M↔N↔O→BR or BR→K↔L↔$M_1$→$M_2$↔N↔O→BR for the kinetics of the bacteriorhodopsin photocycle (13, 31, 32). In particular, the N intermediate plays an important role in the proton pumping process and, at pH 7, achieves a peak population of 30% relative to the peak bleaching of the BR hole (13, 31). Thus in dichroism or anisotropy studies one must consider the effect of absorption by the N intermediate, which overlaps and partially cancels the stronger negative absorption of the BR hole.

## Contributions to the anisotropy decay

It is clear that the anisotropy measured at 550, 570, and 590 nm decays over the 10-ms time scale. Because the measured anisotropy at these wavelengths contains strong contributions from both BR570 and N550, the measured anisotropy cannot be assigned solely to the BR570 hole. It will first be shown that the observed anisotropy decays cannot be attributed to anisotropy decay of the N intermediate, but rather demonstrate that BR570 reorients.

The anisotropy of the BR570 hole can be estimated from the measured anisotropy $r_\lambda(t)$ as follows. From Eqs. 3 and 5, the anisotropy of the BR hole is given by

$$r_{BR}(t) = r_\lambda(t) - \sum_i \frac{\Delta A_\lambda^i(t)}{\Delta A_\lambda^{BR}(t)} [r_i(t) - r_\lambda(t)] \quad (6)$$

where $r_\lambda(t)$ is the measured anisotropy at wavelength $\lambda$, and $r_i(t)$, the anisotropy of the intermediate $i$. The key point here

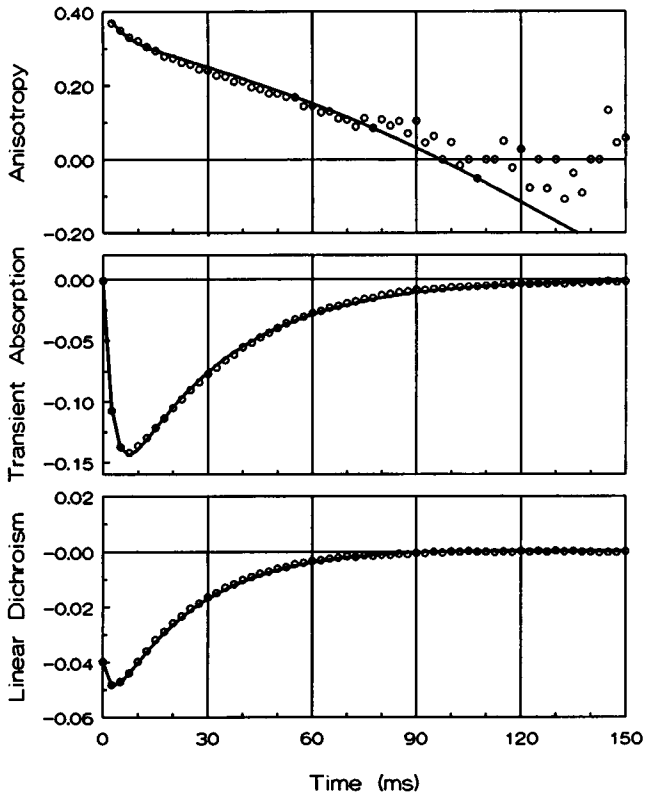


FIGURE 8 Anisotropy (*top*), transient absorption (*center*), and time-resolved linear dichroism (*bottom*) of bacteriorhodopsin measured at 570 nm at 3°C. The solid lines are least-squares fits to the data. The anisotropy and TRLD plots are fit to Eqs. 13 and 14, respectively. The TA data are fit to a double-exponential function (time constants in Table 2).

is that the contribution of the N intermediate to the measured anisotropy decay observed at a given wavelength λ depends on the ratio $-\Delta A_\lambda^N(t)/\Delta A_\lambda^{BR}(t)$ and the difference $r_N(t) - r_\lambda(t)$. Since the peak population of N is ≤ 30% of the initial BR570 bleach at pH 7 (13, 14, 31), and the extinction coefficient of N is smaller than that of BR at 550–590 nm (13), the ratio is less than 0.3. This ratio is smaller in the 550–590-nm region for the other intermediates (M or O) on the millisecond time scale: less than 0.1 for O640 and much smaller for M410 (13). Hence, we are concerned here principally with the N intermediate, although the considerations discussed below apply equally well to other intermediates.

**TABLE 2 Lifetimes of BR at 3°C**

| | λ | $\tau_{LD}$ | $\tau_{TA}$ | $\tau_r$* |
|---|---|---|---|---|
| | nm | ms | ms | ms |
| In water | 410 | 2.5 ± 0.2 | 3.08 ± 0.4 | |
| | | 24.1 ± 0.6 | 28.1 ± 1.0 | 169 |
| | 570 | 2.32 ± 0.08 | 2.74 ± 0.1 | |
| | | 22.2 ± 0.4 | 30.8 ± 0.6 | 80 |
| Fixed with glutaraldehyde | 410 | 5.32 ± 0.4 | 6.48 ± 0.6 | |
| | | 43.5 ± 0.8 | 52.3 ± 1.8 | 258 |
| | 570 | 6.46 ± 0.4 | 7.50 ± 0.6 | |
| | | 47.9 ± 0.6 | 58.4 ± 1.0 | 266 |

* $\tau_r = (1/\tau_{LD} - 1/\tau_{TA})^{-1}$.

The anisotropy difference, $r_N(t) - r_\lambda(t)$, in Eq. 6 must also be considered. Three cases will be discussed. First, if $r_N(t) = r_\lambda(t)$, then the measured anisotropy gives directly the anisotropy decay of the BR570 hole. Clearly, in this case, the data in Figs. 2–4 show that the anisotropy of the BR570 hole decays, and therefore that BR570 must reorient. Second, if $r_N(t)$ is taken to be constant with a value 0.4, the maximum theoretically possible value, then the contribution of N550 to the measured anisotropy at these wavelengths is at most ~0.1 at the peak N concentration. Again, the observed anisotropy requires in this case (and in general for $r_N > r_\lambda$) that the anisotropy of BR570 decays. Third, if $r_N < r_\lambda$, the second term on the right-hand side in Eq. 6 is negative, and $r_{BR}(t) < r_\lambda(t)$. In other words, the effect of a lower value of $r_N(t)$ is to make the measured anisotropy $r_\lambda(t)$ higher than $r_{BR}(t)$, the anisotropy of the BR570 hole. In this circumstance the data show that the anisotropy of BR570 must decay to negative values.

Hence, no matter what the behavior of the anisotropy of N550, it must be concluded from the results observed in Figs. 2–4 that BR570 reorients. It seems most reasonable, however, to suppose that the anisotropy of N550 is constant with a value of ~0.3, since the experimentally determined anisotropies of M410 and O640 are ~0.3, as determined at 410 nm (Fig. 5) and 690 nm (Fig. 6), respectively. In this case, the maximum contribution of N550 to the measured anisotropy at these wavelengths is ~0.1. It follows that the anisotropy decays observed at 550–590 nm are principally due to $r_{BR}(t)$, which decays to a value <0. In contrast, the anisotropies of M410 and O640 remain constant at ~0.3. Clearly, the time dependence of the anisotropy of M410 and O640 is quite different from that of BR570. This constant anisotropy means that, within the limits of these measurements, the monomeric protein does not rotate within the trimeric cell and that the trimeric cell does not rotate with respect to the membrane on this time scale during the photocycle. In addition, no large scale reorientation of the chromophore occurs within the protein during the photocycle.

## Wavelength dependence of the TRLD decay

In order to relate the measured anisotropy $r_\lambda(t)$ to models for reorientation of BR570, we find it convenient first to consider the wavelength dependence of the TRLD decays. The dichroism at any wavelength λ can be conveniently written in the form

$$D_\lambda(t) = \Delta A_\lambda(t) r_i(t) + \Delta A_\lambda^{BR}(t)[r_{BR}(t) - r_i(t)] + \sum_{j \neq i} \Delta A_\lambda^j(t)[r_j(t) - r_i(t)] \quad (7)$$

where $\Delta A_\lambda(t)$ is the total transient absorption at wavelength λ, $\Delta A_\lambda^{BR}(t)$ is the contribution of BR570 to the absorbance changes at this wavelength, $r_i(t)$ is the anisotropy of the intermediate making the strongest contribution to the absorbance changes at λ (e.g., M at 410 nm, N at 550–570 nm, O

at 690 nm), and $j$ labels all other intermediates in the photocycle over the time scale of interest.

The experimental TRLD decays can be fit with Eq. 7, given a model for the time dependence of the anisotropy decay of BR570, $r_{BR}(t)$. The absorbance changes $\Delta A_\lambda(t)$ are given by the TA data at wavelength $\lambda$. The remaining parameters in Eq. 7 can either be determined or approximated. First, $\Delta A_\lambda^{BR}(t)$ is assumed to recover exponentially: the time evolution of $\Delta A_{410}^{BR}(t)$ and $\Delta A_{570}^{BR}(t)$ is taken from the measured recovery at 570 nm, $\Delta A_{570}(t)$ with a time constant of 4 ms at room temperature. This is reasonable because, for times longer than ~1 ms, the time dependence of $\Delta A_{570}(t)$ is essentially the time dependence of the BR570 concentration (13, 31). The time dependence of $\Delta A_{690}^{BR}(t)$ is taken to be given by the decay time of O640. The anisotropies of the M and O intermediates, $r_M(t)$ and $r_O(t)$, are constant within experimental accuracy on this time scale with a value of ~0.3 (Figs. 5 and 6). Since the N intermediate flourishes between the M and O intermediates in the photocycle, the anisotropy of the N intermediate, $r_N(t)$, is also taken to be ~0.3. Given this assumption, the last term in Eq. 7 drops out, and the contributions of all intermediates are contained in the first term. This analysis of the TRLD then includes the contributions from each absorbing species, for example, BR570 and N550 at 570 nm, and BR570 and M410 at 410 nm.

It remains for us to fit the TRLD results to an expression for $r_{BR}(t)$, whose time dependence is determined by the nature of the reorientational motion. A constant value (e.g., $r_{BR}(t) = 0.4$) is not consistent with our results since the recovery time of $D_{570}(t)$ differs markedly from that of $\Delta A_{570}(t)$. In the following section, we consider the time dependence of $r_{BR}(t)$.

## Models for reorientational motion

To account for the anisotropy decay of BR570, we note first that a simple recovery of the initial pigment orientation is not consistent with the anisotropy decay observed at 550, 570, and 590 nm, since at room temperature the membrane rotational diffusion time is much longer than the photocycle time. Hence, the large anisotropy decay in the BR570 hole must be caused by orientational motion of proteins in the trimeric cell that either were not excited by the pump pulse or have completed the photocycle. We have used two models to describe the rotational motion of BR570. The first model assumes that the anisotropy of the BR570 hole can be described simply by an exponential decay. The second model considers possible rotational motion of the two nonphotocycling protein monomers within an excited trimer.

In the first model, we assume that the anisotropy of the BR hole, $r_{BR}(t)$, decays exponentially to zero. Such a decay could result from orientational fluctuations (rotational diffusion) in BR570 that randomize orientations, or from a nonrandom reorientation by ~55°, such as a concerted reorientation of the trimer. This model describes motion of both excited BR570 that has completed the photocycle and the neighboring nonphotocycling BR570, for example, rotation of the trimer within the membrane following completion of the photocycle. (Reorientation of excited BR570 alone upon completion of the photocycle would increase the measured anisotropy at wavelengths where the TA is negative, and is inconsistent with the data in Figs. 2–4.[2]) Fits to the dichroism in Eq. 7 with exponential decay of $r_{BR}(t)$ yield a rotational time of the BR hole at room temperature. Using the same method, we also obtained the rotational time of the BR hole at 550, 590, and 640 nm. The results are shown in Table 3. The rotational time falls in the range of 6–12 ms, about two times longer than the recovery time of BR.

**TABLE 3 Effective rotation time of BR570 at 25°C**

| | λ (nm) | | | | | |
|---|---|---|---|---|---|---|
| | 410* | 550‡ | 570‡ | 590‡ | 640§ | 690¶ |
| $\tau_r^{BR}$(ms) | 9 ± 22 | 13 ± 4 | 7 ± 4 | 11 ± 4 | 12 ± 2 | 7 ± 4 |

*$D(t) = A \exp(-t/2.32\text{ ms}) + B \exp(-t/4\text{ ms}) + C \exp[-t(1/4\text{ ms} + 1/\tau_r^{BR})] + D$.
‡$D(t) = A \exp(-t/\tau_{TA}) + B \exp[-t(1/\tau_{TA} + 1/\tau_r^{BR})] + C$, $\tau_{TA}$ from Table 1.
§$D(t) = A \exp(-t/1.84\text{ ms}) + B \exp(-t/4.81\text{ ms})C \exp[-t(1/4.81\text{ ms} + 1/\tau_r^{BR})] + D$.
¶$D(t) = A \exp(-t/1.24\text{ ms}) + B \exp(-t/5.22\text{ ms}) + C \exp[-t(1/5.22\text{ ms} + 1/\tau_r^{BR}] + D$.

The success of this model can also be judged by its ability to explain the wavelength dependence of anisotropy. Since we have obtained the fitted dichroism and transient absorption, we can produce the theoretical anisotropy by calculating

$$r(t) = D(t)/\Delta A(t) \tag{8}$$

The resulting fits (not shown), are consistent with the early stages of the decay of measured anisotropies (<5 ms) at each wavelength. However, rotational diffusion with a time constant of 6–12 ms, for example of the trimer within the membrane, would also have been detected at 410 (Fig. 5) and 690 nm (Fig. 6), where, on the contrary, a constant anisotropy is observed. Furthermore, random rotational diffusion would cause the anisotropy to decay to zero, but cannot account for a negative anisotropy (positive linear dichroism) measured at 570 and 590 nm. On the other hand, if the reorientational motion is not random, but rather results from a concerted reorientation in the trimer, one must conclude if this model is correct that ground-state BR570 rotates by ≥ 55°, since the anisotropy of BR hole decays to ≤ 0, and neither the photocycling proteins nor the glutaraldehyde-fixed protein were observed to reorient on this time scale. Such a large rotational motion seems unlikely in the well ordered crystalline membrane (11). Hence, in our view the exponential decay model cannot provide a satisfactory description for the rotational motion of proteins in BR membrane. Any model where photocycled BR570 and unexcited BR570 experience the same reorientation would suffer from the same drawback. We therefore view the exponential decay model as merely an empirical description of the rotational motion of BR.

[2] We thank one of the referees for pointing this out.

In the second model for the anisotropy decay of BR570, we take into account the fact that two components can be considered to contribute to the linear dichroism and anisotropy of the BR570 hole. In the trimeric cell, one protein is excited and the other two remain in the ground BR570 state (nonphotocycling or "spectator" proteins) during the photocycle. The spectator proteins have a constant concentration equal to twice the initial concentration of bleached molecules. This leads us to propose a model for reorientational motion of the spectator proteins, which make no contribution to the transient absorption change but can contribute to the linear dichroism and anisotropy if the spectator monomers reorient. Since the system recovers its two-dimensional lattice structure completely after the photocycle (11), the reorientational motion of both photocycling and nonphotocycling proteins must also recover. In other words, the photocycling protein must move back to its original orientation upon completion of the photocycle. In this model, the spectator proteins first change their orientation by a certain angle, and then move back as depicted in Fig. 9. (While both spectator BR monomers are depicted as reorienting in Fig. 9, our analysis applies equally well to reorientation by only one spectator BR.)

In order to test whether this model can account for the anisotropy decays observed at 550–590 nm, we regard the TA and TRLD signals as the sum of two contributions one (negative) from the hole created in the BR570 population by the pump, and the other (positive) from the recovering BR570 population that has completed the photocycle. The first population contributes a constant bleach, $\Delta A_\lambda^{BR}(0)$, to the TA, while the second grows in exponentially as $-\Delta A_\lambda^{BR}(0)[1 - \exp(-t/\tau_{BR})]$, so that

$$\Delta A_\lambda^{BR}(t) = \Delta A_\lambda^{BR}(0)e^{-t/\tau_{BR}} \tag{9}$$

Similarly, the TRLD signal is given by the sum of two contributions,

$$D_\lambda^{BR}(t) = \Delta A_\lambda^{BR}(0)r_h(t) - \Delta A_\lambda^{BR}(0)[1 - e^{-t/\tau_{BR}}]r_e(t) \tag{10}$$

where $r_h(t)$ is the anisotropy of the BR570 hole, and $r_e(t)$ is the anisotropy of the recovered photocycling population. The anisotropy of BR570 is then

$$\begin{aligned} r_{BR}(t) &= D_\lambda^{BR}(t)/[\Delta A_\lambda^{BR}(0)e^{-t/\tau_{BR}}] \\ &= r_e(t) + \Delta r(t)e^{t/\tau_{BR}} \end{aligned} \tag{11}$$

where $\Delta r(t) = r_h(t) - r_e(t)$. The treatment to this point is general, and describes any TRLD experiment where ground state bleach and recovery are measured. At long times, any difference in the anisotropy of the hole and recovering populations is magnified by the diminishing TA signal.

In the present experiments, the anisotropy of the hole is determined by the spectator proteins. In this case, the anisotropy of the BR hole can be written

$$r_h(t) = 0.4 - 2\Delta r_s[1 - \exp(-t/\tau_a)]\exp(-t/\tau_b) \tag{12}$$

where the factor of two comes from the existence of two spectator proteins for each excited monomer, $\Delta r_s = r(\theta + \Delta\theta) - r(\theta)$ is the change of the anisotropy of one of the spectator proteins from orientation $\theta$ to $\theta + \Delta\theta$, and $\tau_a$ and $\tau_b$ are the rotation times for reorientation and return, respectively. (If only one spectator BR reorients, its anisotropy changes by $2\Delta r_s$.) We suppose in this model that the anisotropy of the recovering BR570 population $r_e(t)$ is 0.4, since the photocycling proteins return to their original orientation. From Eqs. 11–12 we obtain the effective anisotropy of the BR570 hole,

$$\begin{aligned} r_{BR}(t) = r_e(t) - \frac{2\Delta A_\lambda^{BR}(0)}{\Delta A_\lambda^{BR}(t)} \\ \times \Delta r_s[1 - \exp(-t/\tau_a)]\exp(-t/\tau_b) \end{aligned} \tag{13}$$

The first contribution, $r_e(t)$, is due to the photoexcited BR, while the second comes from reorientational motion of the spectator proteins. This expression can then be used in Eq.7. The dichroism at 550–590 nm (Eq. 7) can then be rewritten as

$$\begin{aligned} D_\lambda(t) = a\exp(-t/\tau_{BR}) \\ + b[1 - \exp(-t/\tau_a)]\exp(-t/\tau_b) \end{aligned} \tag{14}$$

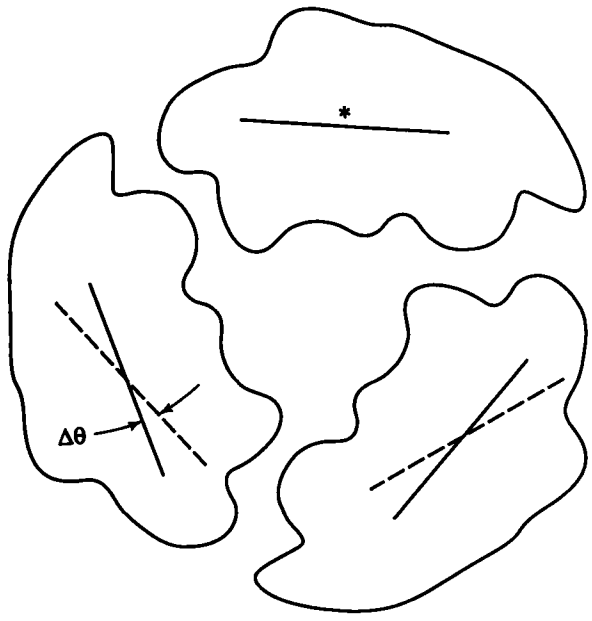


FIGURE 9 Model for reversible reorientation of spectator BR within the trimeric unit cell in purple membrane. The heavy lines represent the location of the retinylidene chromophore in the plane of the membrane. In this model, the photoexcited chromophore (*) returns to its original orientation upon completion of the photocycle. The chromophores in the spectator protein molecules reorient by $\Delta\theta$ to reduce the anisotropy of the BR "hole," and then return to their original orientation. (Although in this representation, both spectator chromophores are depicted as moving, this is not essential to the model. At least one spectator chromophore must move, however.) Chromophore reorientation could result from monomer rotation within the membrane, or from protein conformational motion. (The cross-sectional contour of the BR monomers is based on the x-ray diffraction results from Ref. 16.)

where $a = \Delta A_\lambda^{BR}(0) r_e + [\Delta A_\lambda(0) - \Delta A_\lambda^{BR}(0)] r_N$ is the TRLD at $t = 0$, and $b = -2\Delta A_\lambda^{BR}(0)\Delta r_s$.

A least-squares fit of the dichroism measured at 550, 570, and 590 nm to Eq. 14 yields the notation times $\tau_a$ and $\tau_b$ shown in Table 4. The forward rotation time $\tau_a$ is 1.3–1.9 ms, roughly equal to the decay time of the M410 intermediate (2.1 ms), and the backward rotation time $\tau_b$ is 6.6–8.3 ms, longer than the recover time of the BR hole (4 ms). From the fitted coefficients $a$ and $b$ we can estimate the anisotropy change of $\Delta r_s$,

$$\Delta r_s = \frac{-b}{2a}\left\{ r_e - \frac{[\Delta A_\lambda(0) - \Delta A_\lambda^{BR}(0)]}{\Delta A_\lambda^{BR}(0)} r_N \right\} \quad (15)$$

The ratio $[\Delta A_\lambda(0) - \Delta A_\lambda^{BR}(0)]/\Delta A_\lambda^{BR}(0)$ is the relative contribution of photocycle intermediates and BR570 to the measured TA, and was estimated to be 0.3 at 550–590 nm (from Figs. 2 and 3 in Ref. 13, for $t \sim 2$ ms). With $r_e = 0.4$ and $t_N = 0.3$, we obtain 0.05–0.07 for $\Delta r_s$, as shown in Table 4. The rotation angle is related to the anisotropy by

$$r(\Theta) = \tfrac{1}{5}\langle(3\cos^2\Theta - 1)\rangle \quad (16)$$

where $\langle \cdots \rangle$ represents the orientational average. If the angle between transition dipoles of two proteins is 60° and all spectators rotate by the same angle, then the rotation angle is <8°. Since the transition dipoles are nearly but not exactly parallel to the plane of the membrane (33–36) the actual angle between two transition dipoles is a slightly less than 60° and the rotation angle is slightly smaller.

It may seem odd that whereas the exponential-decay model requires randomization of orientations or a nonrandom reorientation by ≥55°, the reversible rotation model predicts reorientation by <8°. The reason lies in the difference between the anisotropies of the hole and the returning BR570 population, $\Delta r_s$, which is magnified in the measured anisotropy by the decreasing TA signal. In the exponential decay model, however, $\Delta r_s = 0$, and complete randomization of transition-dipole orientations is required for the measured anisotropy to decay to zero. We note that our data also exclude a model where the spectator proteins are immobile, $r_h(t) = 0.4$, while $r_e(t)$ decays. In this case, Eq. 11 predicts that the measured anisotropy cannot decay to zero, even if the orientations of the photoexcited monomers randomize, and at long times will increase above 0.4.

**TABLE 4 Rotational times of the spectator proteins in BR from fitting to the reversible rotation model**

| λ | $\tau_a$ | $\tau_b$ | $b/a$ | $\Delta r_s$ | $\Delta\theta$ |
|---|---|---|---|---|---|
| nm | ms | ms | | | |
| 550* | 1.5 ± 0.4 | 8.3 ± 1.0 | −0.31 | 0.048 | −5.1° |
| 570* | 1.3 ± 1.2 | 6.6 ± 1.2 | −0.46 | 0.071 | −7.4° |
| 590* | 1.9 ± 0.4 | 6.6 ± 0.6 | −0.41 | 0.064 | −6.7° |
| 570‡ | 8.2 ± 1.6 | 16 ± 4 | −0.34 | 0.053 | −5.6° |
| 570§ | 36 ± 50 | 64 ± 160 | −0.24 | 0.037 | −3.9° |
| 570¶ | 7.4 ± 6 | 110 ± 80 | −0.13 | 0.026 | −2.8° |

* In water, pH = 7, 25°C, fitting function:

$$D(t) = ae^{-t/\tau} + b(1 - e^{-t/\tau_a})e^{-t/\tau_b} + c.$$

§Same as in (*) but in 40% glycerol/water mixture.
¶Same as in (*) but in 80% glycerol/water mixture.
In water, pH = 7, 3°C, fitting function:

$$D(t) = \{a\exp(-t/30.8\text{ ms}) + b[1 - \exp(-t/\tau_a)]\exp(-t/\tau_b) + c\exp(-t/2.74\ ms)\}\exp(-t/258\text{ ms}) + d.$$

From the fits to the TRLD and TA scans, as a check of the validity of these parameters, we can calculate the anisotropy according to Eq. (13). The resulting anisotropies plotted in Figs. 2–4 (top panel, *solid line*) are consistent with the measured anisotropies at 550, 570, and 590 nm, respectively, for t<15 ms. (For times longer than ~15 ms the measured anisotropy fluctuates markedly, since the TA and TRLD signals are both within the noise about zero. At long times, as the TA fit decays to zero, the calculated anisotropy must diverge. Noise in the TA and TRLD signals, however, will cause the measured anisotropy at long times to be widely and randomly scattered. For this reason, as discussed earlier, it is preferable to fit the TRLD and TA scans than to fit the anisotropy directly.) The calculated anisotropies show that the spectator reorientation model can account for the BR570 anisotropy decay, without the implausibly large reorientations required by the first model. Note also that this model accounts for the positive linear dichroism at longer times at 570 and 590 nm (Figs. 3 and 4). It should be emphasized, however, that this model and these fits are based on the entire time dependence of the TRLD and TA scans. Because the contribution of the BR570 hole is small for signals measured at 410 and 690 nm, accurate values for the rotational parameters $\tau_a$ and $\tau_b$ cannot be determined from the data at these wavelengths.

We also measured the TA, TRLD, and anisotropy of BR in 40 and 80% glycerol/water solutions at 410, 570, and 640 nm at room temperature. The approximately equal decay times in TA and TRLD at both 410 and 640 nm indicate again that the M and O intermediates have no detectable reorientational motion (Table 1). However, the difference in lifetimes for TA and TRLD at 570 nm clearly shows reorientational motion of BR570. The linear dichroism signals at 570 nm were fit with the model in Eq. 14. The result in glycerol/water mixtures is consistent with those in water. The forward and backward rotational times, as well as the lifetime of the transient absorption, increase as the percentage of glycerol increases (Table 4). The rotational angle is 6 and 4° in 40 and 80% glycerol/water mixtures, respectively. The effect of glycerol on the reorientation time may be related to the reduced activity of water, which has been shown to affect the kinetics of the M intermediate (37). This is consistent with the apparent correlation of the forward reorientation time $\tau_a$ with the lifetime of M410 (Tables 1 and 4). Bulk viscosity could also influence the reorientation times. Further experiments would be required to distinguish between these two effects. The increased viscosity may account for the decreased rotation angle.

At low temperature (3°C), the lifetimes of TA and TRLD in water are different (Table 2) and the anisotropies show a decrease (Figs. 8 and 9) at both 410 and 570 nm. These results imply that the M intermediate as well as BR hole experiences

a rotational motion at low temperature. To account for the rotational motion of BR at low temperature, we also measured the membrane rotational time by glutaraldehyde fixation. The membrane rotational time $\tau_m$ (260 ms) and the measured overall rotational time $\tau_r$ (170 ms) differ at 410 nm. However, these time constants, which are five to 10 times larger than the lifetime $\tau_{TA}$ of M410, are too large to be measured accurately, and probably do not differ significantly. We conclude that the dichroism at 410 nm is adequately described by membrane rotation. Thus, at low temperature, overall membrane rotation can contribute to anisotropy decay during the lifetime of M410, in contrast to the room temperature behavior.

At 570 nm reorientational motion inside the membrane is apparent in addition to the membrane rotation since the rotational time of $\tau_r$ at 570 nm is shorter than at 410 nm (Table 2). We fitted the linear dichroism with an equation similar to Eq. 14 but accounting for the membrane rotation by a factor $e^{-t/\tau_m}$. In the context of the reversible rotation model, the forward and backward rotational times of the spectator proteins were calculated to be 8 and 110 ms, respectively (Table 4). The rotational angle (3°) at low temperature is smaller than at room temperature (8°). Again the calculated anisotropy is consistent with the measured anisotropy (Fig. 8).

We have used a rotation model in which the photocycling proteins have no detectable rotational motion (at room temperature), while the spectator proteins first rotate by some angle during the photocycle in BR, and then move back, to describe the rotational motion of BR. We cannot account for the observed anisotropy decay with a model that does not incorporate rotational motion of spectator BR different from that of recovered photoexcited BR. All of our results are consistent with the reversible rotational model. The forward rotational time $\tau_a$ is shorter than or about equal to the lifetime of the M intermediate, showing that the forward rotational motion probably occurs during the M→N transition. The backward rotational time $\tau_b$ is longer than the lifetime of the BR hole, indicating that the backward rotation happens after the O→BR transition. The reversible rotational motion of BR proteins inside the purple membrane is consistent with recent observations of neutron diffraction (15) and time-resolved x-ray diffraction (16), which show a recovery of crystalline order in the purple membrane upon completion of the photocycle.

### Functional role of rotations

The observation of reorientational motion triggered by light absorption and consequently correlated with the BR photocycle suggests that these reorientational motions might play a functional role in the proton-pumping mechanism of the purple membrane. These motions, however, are not essential to the proton-pumping mechanism, since monomeric BR and BR immobilized in gels are still capable of pumping protons (21, 22). If the reversible rotational model with reorientation of spectator BR monomers is correct, the role of these reorientations may well be related to the puzzling question: what is the role of the trimeric structure of BR in the purple membrane? Evidence for cooperativity in the purple membrane has been reported (38, 39) in the decay kinetics of the M intermediate, suggesting that the photocycle kinetics depend, in the M intermediate, on the state of the neighboring BR. The mechanism by which this cooperativity is transmitted between monomers is not known, but might be related to protein reorientation of spectator BR molecules in response to a protein conformational change or rotation in a photoexcited BR. A similar suggestion has been made by Ahl and Cone (22). Evidence has been found for such conformational changes in the M intermediate (13) or earlier in the photocycle (23).

It is interesting to speculate whether this cooperative conformational motion of the nonphotocycling proteins plays a role in the proton-pumping mechanism. It may be that the formation of the M (or $M_2$, see Refs. 13 and 14) intermediate somehow triggers a small reorientation (<8°) of the neighboring spectator proteins with time constant $\tau_a$. This trigger might be transmitted to the spectator proteins by a small reorientation of the M410 intermediate. Such a reorientation of the chromophore by 11° in the M intermediate has recently been observed in neutron diffraction experiments (40) and might trigger reorientations in neighboring monomers. (Note that anisotropy changes are more sensitive to a given reorientation $\Delta\theta$ when $\theta$ is near 45–60° than when $\theta$ is near 0°. Hence, a comparable reorientation would be more difficult to detect in the anisotropy of M410, than in the anisotropy of spectator protein detected at 570 nm.) The reorientation in the spectator protein might explain the effect of M410 concentration on photocycle kinetics that has been observed (38, 39). Perhaps this cooperative orientational interaction in turn affects the proton-pumping efficiency of the neighboring protein in the trimer.

We thank Sarah A. Mounter for preparation of the bacteriorhodopsin samples and Professor Walther Stoeckenius for the strain of *H. halobium*. We are grateful for helpful discussions with Dr. Christie Brouillette.
This work was supported by grant GM 40071 from the National Institutes of Health.

## REFERENCES

1. Mathies, R. A., S. W. Lin, J. B. Ames, and W. T. Pollard. 1991. From femtoseconds to biology: mechanism of bacteriorhodopsin's light-driven proton pump. *Annu. Rev. Biophys. Biophys. Chem.* 20:491–518.
2. Birge, R. R. 1990. Photophysics and molecular electronic applications of the rhodopsins. *Annu. Rev. Phys. Chem.* 41:683–733.
3. Braiman, M. S., T. Mogi, T. Marti, L. J. Stern, H. G. Khorana, and K. J. Rothschild. 1988. Vibrational spectroscopy of bacteriorhodopsin mutants: light-driven proton transport involves protonation changes of aspartic acid residues 85, 96, and 212. *Biochemistry.* 27:8516–8520.
4. Gerwert, K., G. Souvignier, and B. Hess. 1990. Simultaneous monitoring of light-induced changes in protein side-group protonation, chromophore isomerization, and backbone motion of bacteriorhodopsin by time-resolved Fourier-transform infrared spectroscopy. *Proc. Natl. Acad. Sci. USA.* 87:9774–9778.
5. Fodor, S. P. A., J. B. Ames, R. Gebhard, E. M. M. van den Berg, W. Stoeckenius, J. Lugtenburg, and R. A. Mathies. 1988. Chromophore structure in bacteriorhodopsin's N intermediate: implications for the proton-pumping mechanism. *Biochemistry.* 27:7097–7101.

6. Gerwert, K., B. Hess, J. Soppa, and D. Oesterhelt. 1989. Role of aspartate-96 in proton translocation by bacteriorhodopsin. *Proc. Natl. Acad. Sci. USA.* 86:4943–4947.
7. Otto, H., T. Marti, M. Holz, T. Mogi, M. Lindau, H. G. Khorana, and M. P. Heyn. 1989. Aspartic acid-96 is the internal proton donor in the reprotonation of the Schiff base of bacteriorhodopsin. *Proc. Natl. Acad. Sci. USA.* 86:9228–9232.
8. Braiman, M. S., O. Bousché, and K. J. Rothschild. 1991. Protein dynamics in the bacteriorhodopsin photocycle: submillisecond Fourier transform infrared spectra of the L, M, and N photointermediates. *Proc. Natl. Acad. Sci. USA.* 88:2388–2392.
9. Smith, S. O., J. A. Pardoen, P. P. J. Mulder, B. Curry, J. Lugtenburg, and R. Mathies. 1983. Chromophore structure in bacteriorhodopsin's $O_{640}$ photointermediate. *Biochemistry.* 22:6141–6148.
10. Holz, M., L. A. Drachev, T. Mogi, H. Otto, A. D. Kaulen, M. P. Heyn, V. P. Skulachev, and H. G. Khorana. 1989. Replacement of aspartic acid-96 by asparagine in bacteriorhodopsin slows both the decay of the M intermediate and the associated proton movement. *Proc. Natl. Acad. Sci. USA.* 86:2167–2171.
11. Henderson, R., J. M. Baldwin, T. A. Ceska, F. Zemlin, E. Beckmann, and K. H. Downing. 1990. Model for the structure of bacteriorhodopsin based on high-resolution electron cryo-microscopy. *J. Mol. Biol.* 213: 899–929.
12. Braiman, M. S., P. L. Ahl, and K. J. Rothschild. 1987. Millisecond Fourier-transform infrared difference spectra of bacteriorhodopsin's $M_{412}$ photoproduct. *Proc. Natl. Acad. Sci. USA.* 84:5221–5225.
13. Váró, G., and J. K. Lanyi. 1991. Kinetic and spectroscopic evidence for an irreversible step between deprotonation and reprotonation of the schiff base in the bacteriorhodopsin photocycle. *Biochemistry.* 30: 5008–5015
14. Váró, G., and J. K. Lanyi. 1991, Thermodynamics and energy coupling in the bacteriorhodopsin photocycle. *Biochemistry.* 30:5016–5022.
15. Dencher, N. A., D. Dresselhaus, G. Zaccai, and G. Büldt. 1989. Structural changes in bacteriorhodopsin during proton translocation revealed by neutron diffraction. *Proc. Natl. Acad. Sci. USA.* 86:7876–7879.
16. Koch, M. H. J., N. A. Dencher, D. Oesterhelt, H.-J. Plöhn, G. Rapp, and G. Büldt. 1991. Time-resolved X-ray diffraction study of structural changes associated with the photocycle of bacteriorhodopsin. *EMBO J.* 10:521–526.
17. Subramaniam, S., T. Marti, S. J. Rösselet, K. J. Rothschild, and H. G. Khorana. 1991. The reaction of hydroxylamine with bacteriorhodopsin studied with mutants that have altered photocycles: selective reactivity of different photointermediates. *Proc. Natl. Acad. Sci. USA.* 88:2583–2587.
18. Lozier, R. H., and W. Niederberger. 1977. The photochemical cycle of bacteriorhodopsin. *Fed. Proc.* 36:1805–1809.
19. Sherman, W. V., and S. R. Caplan. 1977. Chromophore mobility in bacteriorhodopsin. *Nature.* 265:273–274.
20. R. E. Godfrey. 1982. Photoselection and circular dichroism in the purple membrane. *Biophys. J.* 38:1–6.
21. Czégé, J., A. Dér, L. Zimányi, and L. Keszthelyi. 1982. Restriction of motion of protein side chains during the photocycle of bacteriorhodopsin. *Proc. Natl. Acad. Sci. USA.* 79:7273–7277.
22. Ahl, P. L., and R. A. Cone. 1984. Light activates rotations of bacteriorhodopsin in the purple membrane. *Biophys. J.* 45:1039–1049.
23. Wan, C., J. Qian, and C. K. Johnson. 1991. Conformational motion in bacteriorhodopsin: the K to L transition. *Biochemistry.* 30:394–400.
24. Der, A., S. Száraz, and J. Czégé. 1988. Orientation of the chromophore plane in purple membrane. *Biophys. J.* 54:1175–1178.
25. Otto, H., and M. P. Heyn. 1991. Between the ground- and M-state of bacteriorhodopsin the retinal transition dipole moment tilts out of the plane of the membrane by only 3°. *FEBS Lett.* 293:111–114.
26. Wan, C., J. Qian, and C. K. Johnson. 1990. Time-resolved polarization study of anisotropy in bacteriorhodopsin. *J. Phys. Chem.* 94:8417–8423.
27. Johnson, C. K., J. M. Bostick, S. A. Mounter, K. L. Ratzlaff, and D. E. Schloemer. 1988. Picosecond time-resolved laser spectrometer with expanded delay range. *Rev. Sci. Instrum.* 59:2375–2379.
28. Oesterhelt, D., and W. Stoeckenius. 1974. Isolation of the cell membrane of *Halobacterium halobium* and its fractionation into red and purple membrane. *Methods Enzymol.* 31:667–678.
29. Cantor, C. R., and P. R. Schimmel. 1980. Biophysical Chemistry, Part II. Freeman, New York. pp. 461 and 557–565.
30. *CRC Handbook of Chemistry, and Physics*, 51st. ed. 1970. R. C. Weast, ed. The Chemical Rubber Co., Cleveland, OH. p. F-36.
31. Ames, J. B., and R. A. Mathies. 1990. The role of back-reactions and proton uptake during the N → O transition in bacteriorhodopsin's photocycle: a kinetic resonance Raman study. *Biochemistry.* 29:7181–7190.
32. Nagle, J. F. 1991. Photocycle kinetics: analysis of raman data from bacteriorhodopsin. *Photochem. Photobiol.* 54:897–903.
33. Heyn, M. P., R. J. Cherry, and U. Müller. 1977. Transient and linear dichroism studies on bacteriorhodopsin: determination of the orientation of the 568 nm all-*trans* retinal chromophore. *J. Mol. Biol.* 117: 607–620.
34. Bogomolni, R. A., S.-B. Hwang, Y.-W. Tseng, G. I. King, and W. Stoeckenius. 1977. Orientation of the bacteriorhodopsin transition dipole. *Biophys. J.* 17:98*a*. (Abstr.)
35. Korenstein, R., and B. Hess, 1978. Immobilization of bacteriorhodopsin and orientation of its transition moment in purple membrane. *FEBS Lett.* 89:15–20.
36. Huang, J. Y., and A. Lewis. 1989. Determination of the absolute orientation of the retinylidene chromophore in purple membrane by a second-harmonic interference technique. *Biophys. J.* 55:835–842.
37. Cao, Y., G. Váró, M. Chang, B. Ni, R. Needleman, and J. K Lanyi. 1991. Water is required for proton transfer from aspartate-96 to the bacteriorhodopsin Schiff base. *Biochemistry.* 30:10972–10979.
38. Korenstein, R., B. Hess, and D. Kuschmitz. 1978. Branching reactions in the photocycle of bacteriorhodopsin. *FEBS Lett.* 93:266–270.
39. Korenstein, R., and B. Hess. 1982. Cooperativity of photocycle in purple membrane. *Meth. Enzym.* 88:193–201.
40. Haub, T., M. P. Heyn, G. Buldt, and N. A. Dencher. 1993. *Biophys. J.* 64:A213.